Wave propagation in acoustic ducts with periodic side branch resonators

Flaianny B. Pacheco, Brenno V. L. Campos, José Maria C. Dos Santos

Computational Mechanics Dept, University of Campinas
Rua Mendeleiev, 200, Cidade Universitária "Zeferino Vaz", Barão Geraldo, CEP 13083-860, Campinas (SP), Brazil
flaiannypacheco@gmail.com, brenno.campos@fem.unicamp.br, zema@unicamp.br

Abstract. This paper presents the behavior of an acoustic duct with periodic side branch tube resonators commonly used as a noise control device, which can be tuned to enlarge the resonance bandwidth and improve the transmission loss. An interesting approach to obtain a broader attenuation range in a duct consists in to distribute side branches tubes resonators periodically along the duct. This generates some frequency bands, known as bandgaps, where harmonic waves do not propagate. Bandgaps are generated based on the special frequency of mismatched impedance areas which produce Bragg scattering (destructive acoustic interference) and local resonance effects from the duct-tube system. This work investigates bandgaps created in duct-tube system using acoustic transfer matrix method and finite element models. Numeric results are presented as dispersion diagrams, sound pressure level and transmission loss. These results are discussed and compared with each other. Periodic geometry variations of the side tubes are also investigated.

Keywords: side branch, metamaterials, bandgaps, acoustic system

1 Introduction

In the last 20 years, theoretical and experimental studies have been developed on applications of periodic structures such as acoustic phononic crystals and metamaterials for passive noise control [1]. Acoustic metamaterials are composed by a set of resonators distributed periodically (or not) in space, where the local resonance effect generates stop bands or bandgaps. If distribute periodically along the space, they also produce Bragg-type stop bands, which are generated by impedance mismatch (Bragg scattering) [2, 3]. Acoustic resonators have been used for sound control in many engineering applications, such as internal combustion engines, compressors, ventilation systems, etc. They can be classified as active and passive noise controls. In passive silencers the sound is attenuated based on its capacity to reflect and absorb the acoustic energy. Active silencers uses feedback control approach using electronic devices to attenuate the sound [4]. Acoustic metamaterials based on local resonators have been studied as an application of band-rejected filter for noise control. One of them, is the closed side-branch tube resonator, which is composed by a set of close tubes connected along a main duct [5]. It can generate larger bandgaps with the transmission loss improvement. This work investigates bandgaps created in a metamaterial side branch tube-duct using acoustic transfer matrix method (TMM) verified by finite element method (MEF). Numeric results are presented as dispersion diagrams, sound pressure level and transmission loss. These results are discussed and compared with each other. Periodic geometry variations of the side branch tubes are also investigated.

Figure 1 shows a scheme of periodic acoustic metamaterial side-branch tube-duct, emphasizing the unit-cell (*contour*) including the main dimensions: unit-cell length (L), duct diameter (D), side-branch tube diameter (d) and length (l).

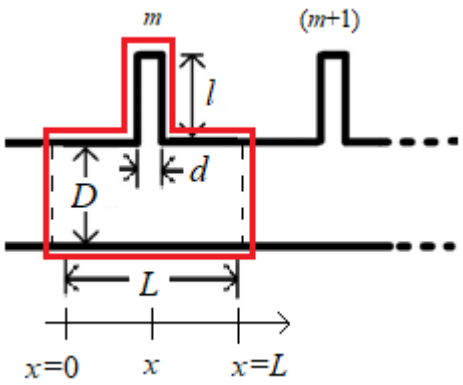

Figure 1. Scheme of a periodic duct with side-branch tube resonators emphasizing a unit-cell (*contour*).

2 Acoustic Metamaterial Modeling

The Transfer Matrix Method (TMM) has been widely used to calculate and optimize acoustic systems [6]. The metamaterial side-branch tube-duct unit-cell is composed by three coupled ducts, which can be modeled using the duct TMM model. From the unit-cell (*contour*) in Fig. 1, let's assume U_x and p_x as volume velocity and acoustic pressure at the space point x, respectively. Then, the relationship between states at the unit-cell (inlet) left-side hand ($x = 0$) and at the unit-cell (outlet) right-side hand ($x = L$) can be formulated as [7]::

$$\left\{ \begin{array}{c} U_0 \\ p_0 \end{array} \right\} = \underbrace{\left[\begin{array}{cc} cos(\hat{k}l_e) & j\frac{S_d}{\rho c} sin(\hat{k}l_e) \\ j\frac{\rho c}{S_d} sin(\hat{k}l_e) & cos(\hat{k}l_e) \end{array} \right]}_{\mathbf{T}_D} \left\{ \begin{array}{c} U_L \\ p_L \end{array} \right\}, \tag{1}$$

where S_d is the cross section area of the duct, ρ is the air mass density and c is the air sound velocity. The $\hat{k} = k(1 + j\eta)$ is the complex wave number that has been formulated to include air dissipation, where $k = \omega/c$ is the wavenumber, η is the loss factor and ω is the circular frequency. Also, $l_e = L + 0.6(D/2)$ is the duct effective length including the correction factor for the unflanged-end condition. From the Eq. (1) the duct transfer matrix is defined as $\mathbf{T}_D$.

The unit-cell model (*contour*) in Fig. 1 is the coupling between three acoustic ducts (duct half-left, side-branch tube and duct half-right) at the point x.

$$\begin{aligned} U_0(x) &= U_{SB}(x) + U_L(x), \\ p_0(x) &= p_{SB}(x) = p_L(x). \end{aligned} \tag{2}$$

Rewriting Eq. (2) in matrix form it has:

$$\left\{ \begin{array}{c} U_0 \\ p_0 \end{array} \right\} = \left[\begin{array}{c} U_{SB} + U_L \\ p_L \end{array} \right] = \left[\begin{array}{cc} 1 & U_{SB}/p_L \\ 0 & 1 \end{array} \right] \left\{ \begin{array}{c} U_L \\ p_L \end{array} \right\}. \tag{3}$$

From Eq. (2), $p_L(x) = p_{SB}(x)$, then in Eq. (3)) the matrix element $U_{SB}/p_L = U_{SB}/p_{SB} = 1/Z_{SB}$, where Z_{SB} is the side branch tube resonator acoustic impedance, and Eq. (3) becomes:

$$\left\{ \begin{array}{c} U_0 \\ p_0 \end{array} \right\} = \underbrace{\left[\begin{array}{cc} 1 & 1/Z_{SB} \\ 0 & 1 \end{array} \right]}_{\mathbf{T}_{SB}} \left\{ \begin{array}{c} U_L \\ p_L \end{array} \right\}, \tag{4}$$

where $\mathbf{T}_{SB}$ is the side-branch tube resonator transfer matrix. Writing the left state vector as $\mathbf{q}_{\text{L}} = \{U_0 \;\; p_0\}^T$, the

right state vector as $\mathbf{q}_{\mathtt{R}} = \{U_L \;\; p_L\}^T$, and coupling the three acoustic elements, it has:

$$\mathbf{q}_{\mathtt{L}} = \mathbf{T}_{D_1}\mathbf{T}_{SB}\mathbf{T}_{D_2}\mathbf{q}_{\mathtt{R}} = \underbrace{\begin{bmatrix} A & B \\ C & D \end{bmatrix}}_{\mathbf{T}} \mathbf{q}_{\mathtt{R}} \tag{5}$$

where $\mathbf{T}_{D_1}$ and $\mathbf{T}_{D_2}$ are the duct half-left and half-right transfer matrices, respectively, and $\mathbf{T}$ is the metamaterial side-branch tube resonator-duct uni-cell transfer matrix.

From the Eq. (5)) the acoustic pressure response at the duct position $x = L$ to a volume velocity excitation at $x = 0$ can be obtained as [8]:

$$\frac{p_L}{U_0} = \frac{Z_R}{A + BZ_R}. \tag{6}$$

where Z_R is the radiation impedance at the unflanged open output end of the duct.

The Transmission Loss (TL) can be described as the difference between the sound power before the silencer and the sound power that continues to be transmitted after the silencer. According to Munjal [7], the TL is not dependent on the source, and by taking anechoic terminations it can be obtained as:

$$TL = 20\log_{10}\left|\frac{A + \frac{S_d}{\rho c}B + \frac{\rho c}{S_d}C + D}{2}\right|. \tag{7}$$

Consider consecutive unit cells, m and $m+1$, in the acoustic metamaterial as shown in Fig 1. By applying it into the Eq. (5) the unit-cell compatibility and continuity conditions, $\mathbf{q}_{\mathtt{R}}{}^{(m)} = \mathbf{q}_{\mathtt{L}}{}^{(m+1)}$. Using the Bloch-Floquet theorem for an infinity numbers of unit-cells, $\mathbf{q}_{\mathtt{L}}{}^{(m+1)} = e^{\mu}\mathbf{q}_{\mathtt{L}}{}^{(m)}$. Abandoning the super- and sub-scripts in the equations, the Bloch wave eigenproblem can be obtained as:

$$[\mathbf{T} - \mathbf{I}e^{\mu}]\mathbf{q} = \mathbf{0} \tag{8}$$

where $\mathbf{I}$ is the identity matrix, $\mu = -jkL$ is the attenuation constant, k is the Bloch wavenumber and $\mathbf{q}$ is the Bloch wave mode.

3 Results and Discussion

In order to validate the computational implementation of the Transfer Matrix Method (TMM) code in Matlab software, two examples are performed and compared with the results obtained by the Finite Element Method (FEM) with the commercial ANSYS ® software. Simulated models are side-branch tube resonator-duct metamaterial with one unit cell and three unit-cells. For all simulated examples the geometry and air properties are as shown in Table 1. The metamaterial transmission loss are calculated by FEM using ANSYS 3D model with the

Table 1. Geometry and air properties.

Geometry/Property	Value
Unit-cell length (L)	0.342 m
Duct diameter (D)	0.15 m
Tube diameter (d)	0.075 m
Tube length (l)	0.342 m
Air sound velocity (c)	343.24 m/s
Air mass density (ρ)	1.2041 kg/m^3

FLUID30 element type. Using the mesh-free option the metamaterial model with one unit-cell was meshed with

22,111 elements and 4,423 nodes, while the three unit-cells metamaterial model was meshed with 57,464 elements and 11,332 nodes. Figure 2 shows FEM meshes for the side-branch tube resonator-duct metamaterial with one and three unit-cells.

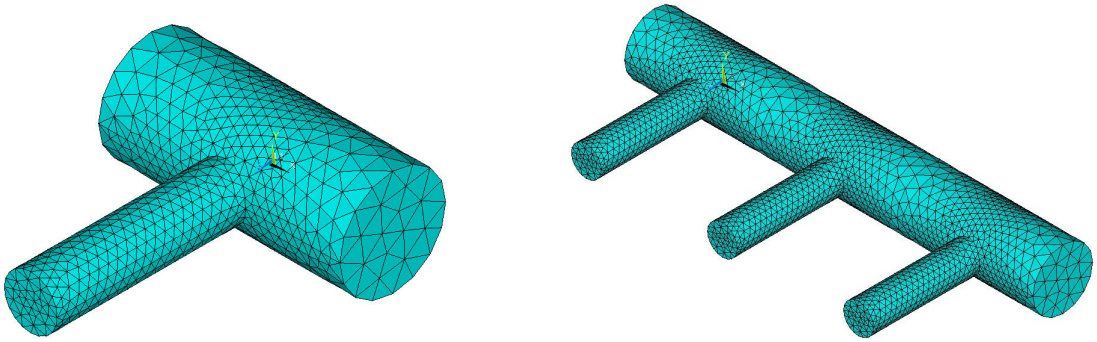

(a) N=1 cell (b) N=3 cells

Figure 2. FEM meshes for the side-branch tube resonator-duct metamaterial with: a) N=1 cell; b) N=3 cells.

Figure 3 shows the mean transmission loss ($\overline{TL} = TL/N$) results calculated by TMM (Matlab) and FEM (Ansys) for the side-branch tube resonator-duct metamaterial with one and three unit-cells. It can be seen that the results calculated by both methods presents good agreement verifying the implemented TMM code.

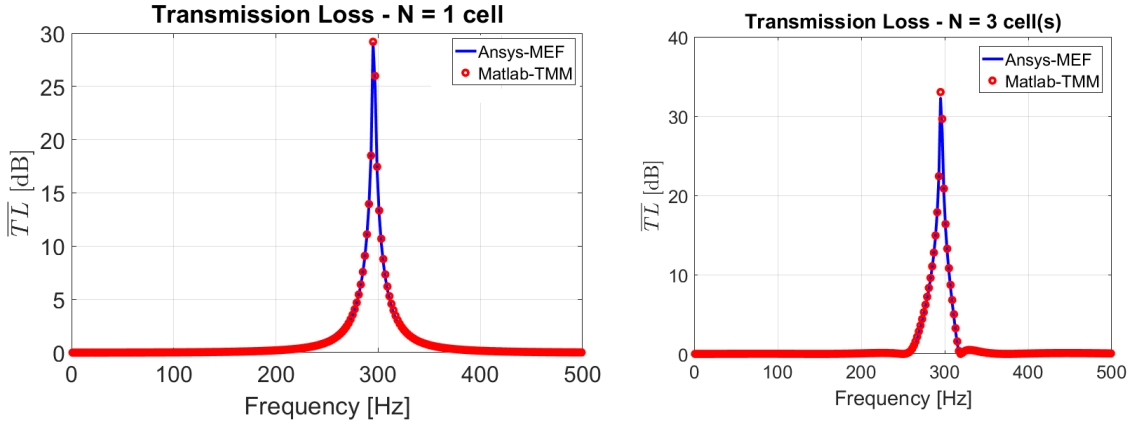

(a) N=1 cell (b) N=3 cells

Figure 3. Comparison of $\overline{TL}$ calculated by FEM (Ansys) and TMM (Matlab) for the side-branch tube resonator-duct metamaterial with: a) N=1 cell; b)N=3 cells.

Based on a try-and-error parameter sensitivity analysis, it was founded that the most sensitive parameters to change the bandgp location and width generated by the side-branch tube-duct metamaterial are the unit-cell (L) and side-branch tube (l) lengths. Defining the length ratio $\beta = l/L$, dispersion diagrams calculated by TMM for $\beta = \{1/5, 1/4, 1/2, 1/3, 2/3, 4/5\}$ are performed and the results are presented in Figure 4.

All dispersion diagram plots presents the real part (*top*) and the negative imaginary part (*bottom*) of non-dimensional Bloch wavenumber (kL) versus frequency in Hz. Bragg type (BT) bandgaps can be identified in frequency bands where $\Re\{kL\} = \pi \vee 0$ (Bragg limit) and $-\Im\{kL\} \neq 0$ (evanescent waves), while Local Resonance (LR) type bandgaps can be identified by a discontinuity in the $\Re\{kL\}$ coincident with a peak in the $-\Im\{kL\}$, located at the first resonance frequency of the side-branch tube ($f_n = c_0(n-0.5)/2l, \;\; n = 1, 2, \ldots$).

In the Fig. 4(a) dispersion diagram for $\beta = 1/2$ (*solid line*) is shown, where the BT bandgaps can be identified around the frequency bands of 445-501 Hz, 1,003-1,048 Hz and 1,800- over 2,000 Hz, while only one LR bandgap appears around the frequency bands of 682-772 Hz, with the $-\Im\{kL\}$ peak at the resonance frequency of side-branch tube ($f_1 = 721$ Hz). A similar behavior occurs for $\beta = 1/3$ (*solid line*), where BT bandgaps are identified around the frequency bands of 478-501 Hz, 934-1.002 Hz while one LR bandgap occurs around the 1265-1417 Hz with the $-\Im\{kL\}$ peak at the resonance frequency of side-branch tube ($f_1 = 1{,}386$ Hz). It can be noticed

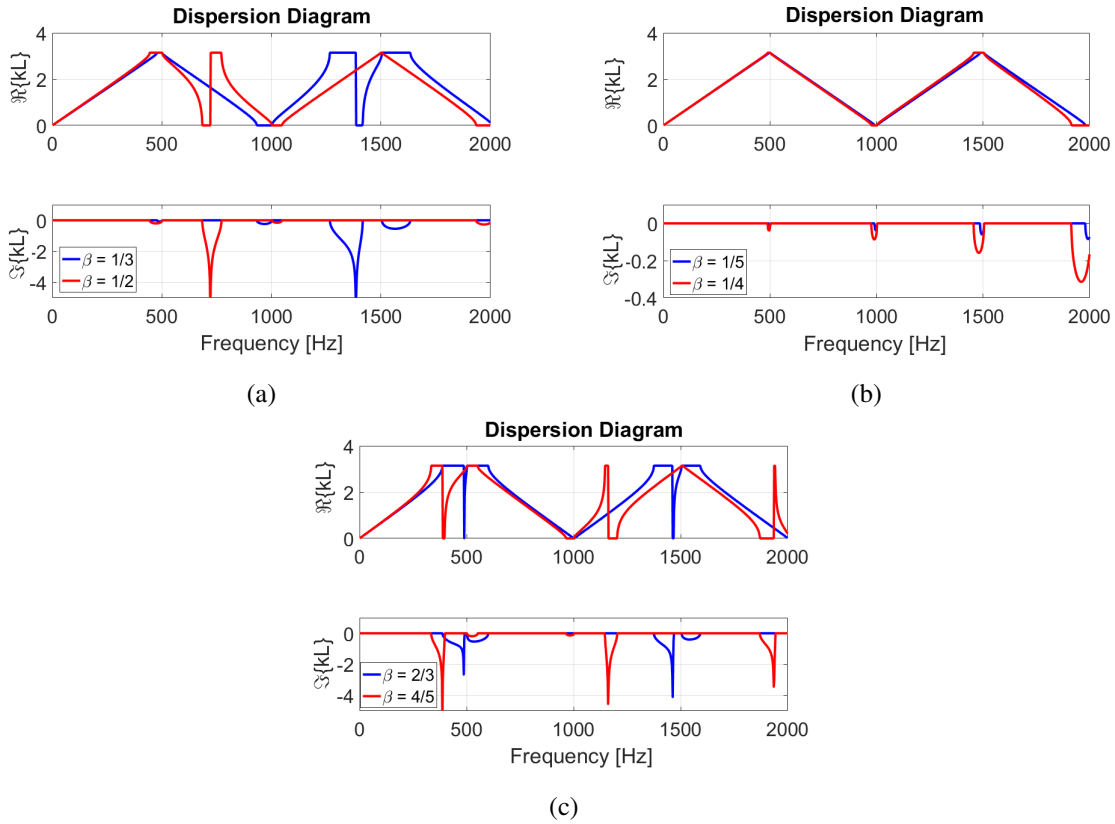

Figure 4. Dispersion diagram calculated by TMM (Matlab) for the side-branch tube resonator-duct metamaterial with: a) β = 1/2 and 1/3; b)β = 1/5 and 1/4; c)β = 2/3 and 4/5.

that reducing β from 1/2 para 1/3, which means decreases side-branch length (l) relate to the unit-cell length (L), the LR bandgap is shifted for a higher frequency band and a larger bandgap width is obtained. However, for the BT bandgaps a shift for higher or lower frequency band is observed, while the bandgap width can be enlarged or diminished.

In the Fig. 4(b) dispersion diagram for β = 1/4 (*solid line*) and 1/5 (*solid line*) are shown and present similar behavior. For both β three complete and one partial BT bandgaps are identified in the analyzed frequency band, close to the same bandgap as the first cases (around 0.5, 1.0, 1.5 and 2.0 kHz), with some bandgap width enlargements and higher attenuation as the frequency band increases. For this case β is being reduced even more related to the first cases, which means l even smaller then the unit-cell length (L). Based on the behavior of first cases, it can be seen that no LR bandgaps appears in the analyzed frequency band, since they were shifted to higher frequency bands. From these results it is noticed that by reducing even more β the LC resonance frequency becomes high and moves de bandgap to higher frequency bands, while the BT badgaps do not changes noticeably its position in frequency, but its band width and attenuation level change substantially.

In the Fig. 4(c) dispersion diagram for β = 2/3 and 4/5 are presented, which means side-branch tube length (l) larger then the unit-cell length (L). For β = 2/3 (*solid line*) apparently there is only one BT bandgap around 1.0 kHz and two LR bandgaps around the first and second side-branch tube resonance frequency. However, here occurs a strong BT and LR bandgap coupling, since LR resonance frequencies (side-branch tube resonance frequency) are close to the BT resonance frequencies ($f_{b_n} = nc_0/2L, \quad n = 1, 2, \ldots$), which for the first bandgap are f_1 = 487.6 Hz and f_{b_1} = 501.5 Hz, and for the third band gap are f_2 = 1,462.7 Hz) and f_{b_3} = 1,504.4 Hz. For β = 4/5 (*solid line*) there are three BT bandgaps (around 0.5 1.0 and 1.5 kHz) and three LR bandgaps around the first, second and third side-branch tube resonance frequency, without coupling between BT and LR bandgaps.

A harmonic analysis in the frequency range of 0-500 Hz is performed, considering a unitary volume velocity excitation at the entrance of the duct ($x = 0$) and acoustic pressure response at the duct output ($x = L$) considering anechoic boundary conditions (without reflection) at both ends. Figure 5 shows the forced response for side branch tube resonator system calculated by TMM (Matlab) and FEM (Ansys). This is a preliminary result, where the curves of TMM and FEM are not in total agreement. There are some issues related to the FEM simulation with Ansys that needs to be solved. It is expected to present a better result for this comparison until the conference.

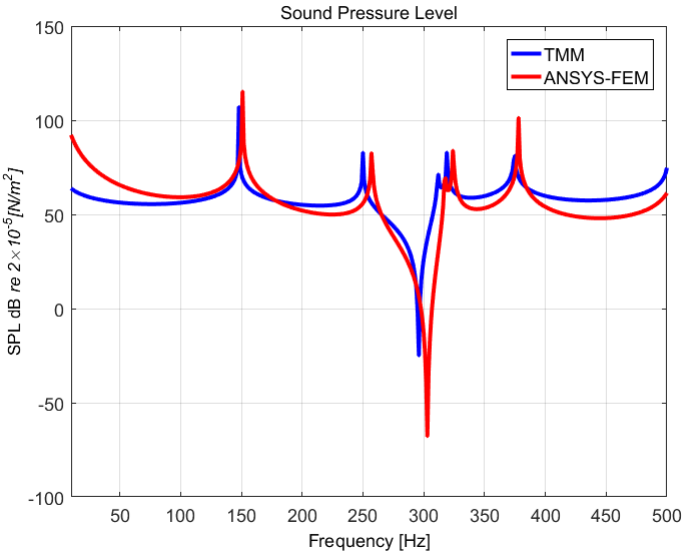

Figure 5. Sound pressure level of side branch tube resonator.

4 Conclusions

Based on the results and studies available in the literature, it is concluded that the methodology used to assess sound attenuation can help to optimize noise control in other acoustic devices.

The comparison of transmission loss results between the results obtained by the finite element method, using the Ansys software, and the transfer matrix method confirms the reliability of the TMM at low frequency bands.

Changing the length of the side-branch tube resonator interferes with the bandgap position, width and attenuation level generated by locally resonant and periodicity.

Acknowledgements. The authors are thankful to FAPEMA (Grant Nos. BD-08741/17 and BM-08714/17), FAPESP (Grant No. 2018/15894-0), and CNPq (Grant No. 313620/2018) for the financial support.

Authorship statement. The authors hereby confirm that they are the sole liable persons responsible for the authorship of this work, and that all material that has been herein included as part of the present paper is either the property (and authorship) of the authors, or has the permission of the owners to be included here.

References

[1] M. Farooqui, T. Elnady, and W. Akl. Sound attenuation in ducts using locally resonant periodic aluminum patches. *The Journal of the Acoustical Society of America*, vol. 139, n. 6, pp. 3277–3287, 2016.

[2] M. I. Hussein, M. J. Leamy, and M. Ruzzene. Dynamics of phononic materials and structures: Historical origins, recent progress, and future outlook. *Applied Mechanics Reviews*, vol. 66, n. 4, 2014.

[3] A. R. C. d. Sousa and others. Modelagem de metamaterial acústico para absorção sonora em baixas frequências, 2017.

[4] R. F. Barron. *Industrial noise control and acoustics*. CRC Press, 2002.

[5] X. Wang, W. Zhu, and Y. Zhou. Sound transmission in a duct with a side-branch tube array mounted periodically. *The Journal of the Acoustical Society of America*, vol. 139, n. 6, pp. 202–208, 2016.

[6] L. Beranek and I. Vér. *Noise and vibration control engineering: principles and application*. Wiley Interscience, 1992.

[7] M. L. Munjal. *Acoustics of ducts and mufflers with application to exhaust and ventilation system design*. John Wiley & Sons, 1987.

[8] S. Singh, C. H. Hansen, and C. Q. Howard. A detailed tutorial for evaluating in-duct net acoustic power transmission in a circular duct with an attached cylindrical helmholtz resonator using transfer matrix method. In *Acoustics 2008*, Victoria, Australia, 2008.